BEAM INTERACTIONS WITH MATERIALS AND ATOMS

Full length article

Multiple scattering of 855 MeV electrons in amorphous and crystalline silicon: Simulations versus experiment

Germán Rojas-Lorenzo [a], Jesús Rubayo-Soneira [a],*, Maykel Márquez-Mijares [a], Andrei V. Korol [b], Andrey V. Solov'yov [b]

[a] *Instituto Superior de Tecnologías y Ciencias Aplicadas, Universidad de La Habana (InSTEC-UH), Ave. Salvador Allende 1110, Plaza de la Revolución, Havana, 10400, Cuba*
[b] *MBN Research Center, Altenhöferallee 3, Frankfurt am Main, 60438, Germany*

ARTICLE INFO

ABSTRACT

The angular distribution function of multiple scattering experienced by 855 MeV electrons passing through an amorphous silicon plate and an oriented silicon crystal has been studied by means of relativistic molecular dynamics simulations using two types of the potentials that describe electron–atom interaction. The differences in the angular distributions of the beam particles in both media are analyzed. The results obtained are compared to the experimental data and to the results of Monte Carlo simulations.

1. Introduction

In the 1960s, Lindhard published a comprehensive theoretical study on the influence of crystal structure on the motion of energetic charged particles [1]. He revealed and described directional effects for the projectiles incident on oriented crystals which lead to the governed motion due to inhomogeneity, anisotropy and lack of randomness in the medium. By introducing the concept of the continuous potential of an atomic string or plane in a crystal Lindhard explained the channeling phenomenon (i.e. the guided motion of charged projectiles in the vicinity of major crystallographic axis or planes) that had been detected earlier in the experiments on propagation lengths for heavy ions in aluminum [2]. Since then studies of the channeling phenomenon, or more generally, of passage of ultra-relativistic particles through oriented crystals of different geometry (linear, bent, periodically bent crystals) have expanded to form a broad field of theoretical and experimental research (see, e.g., [3]) as well as of a number of applications. The latter include, for example, beam manipulation, – steering, focusing, collimation, splitting, and extraction, by means of crystals (see, e.g., Refs. [4–8] and references therein). Another promising potential application concerns realization of novel intensive gamma-ray light sources operating at photon energies within MeV–GeV range that can be constructed by exposing oriented crystals to beams of ultra-relativistic charged projectiles [9–11].

Regularity in positions of crystal constituents modifies multiple scattering and radiative processes for a charged projectile particle as compared to its passage through an amorphous medium [12]. This occurs for the channeling particles as well as for those experiencing the over-barrier motion, i.e. moving across crystal planes/axes.

Recently, an experimental observation was reported [13] of the reduction of multiple scattering for high-energy positively charged particles experiencing planar channeling in single crystals. The measurements have shown that the root-mean-square planar angle of multiple scattering in the plane normal to the plane of the channeling is less than that for the over-barrier particles in the same crystal. The explanation presented refers to the specific feature of the channeling phenomenon of positively charged projectiles. Their interaction with the crystal atoms is repulsive, therefore, in the planar regime they channel in between two adjacent planes. If the amplitude of the channeling oscillations is smaller than $d/2 - a_{\mathrm{TF}}$ (d is the interplanar distance and a_{TF} is the Thomas–Fermi radius of the atom) then channeling occurs in the spatial region with the electron volume density less (on average) than in the amorphous medium. As a result, such particles can penetrate large distance into a crystal and exit from the crystal at relatively small scattering angle.

In another recent experiment [14] carried out at the Mainz Mikrotron (MAMI) facility the observation has been made of the reduction of multiple scattering angle of electrons in a crystalline silicon target as compared to that in an amorphous target of the same mass thickness. It is indicated in the cited paper that a projectile particle while moving in a crystalline environment can interact either with

---

individual atoms as in an amorphous medium (incoherent scattering) or with atoms arranged in strings or in planes (coherent scattering). Section 2 in Ref. [14] provides quantitative analysis of the conditions to be met for the incident angle of particle's momentum $\vec{p}_0$ with respect to the axis (plane) that facilitate the coherent scattering and, as a result, lead to the decrease in the scattering angle. The effect of coherent scattering suppression (CSS) that occur at certain crystal orientations has been observed experimentally as well as modeled via Monte Carlo simulations [15].

In this paper we present an independent analysis of the multiple scattering process of electrons in the crystalline and amorphous silicon targets. The analysis is based on the results of the relativistic classical molecular dynamics simulations performed by means of the MBN Explorer package [16–19]. The parameters of the targets as well as the characteristic of the electron beam (energy and angular divergence) used in the simulations correspond to those used in the experiment [14] (see Section 2 for details). In Section 3 the numerical results obtained are compared with the experimental data collected at MAMI. In Section 4, some conclusions of this work are summarized and future perspectives are presented.

2. Methodology

A number of numerical tools have been developed within frameworks of different theoretical approaches to simulate various phenomena occurring during passage of ultra-relativistic projectiles through oriented crystals and amorphous solids (see Ref. [20] for and overview of the most recent ones). In many cases, a rigorous description can be achieved within the classical formalism by considering particles' trajectories. For numerical modeling of channeling and related phenomena beyond the continuous potential framework we utilize the multi-purpose computer package MBN Explorer [16,17,19,21] and a supplementary special multitask software toolkit MBN Studio [18]. Developed originally as a universal program for investigating structure and dynamics of molecular systems at various spatial scales, ranging from nanometers and beyond, the package allows for a computation of relativistic projectile motion in various environments including crystalline structures [21]. The simulation procedure accounts for the interaction of a projectile particle with all atoms in the environment. A number of various interatomic potentials implemented in the package enables rigorous simulations of different media. The package serves as a powerful numerical tool to explore relativistic dynamics in crystals and amorphous systems. Its efficiency and reliability have been evaluated for channeling of ultra-relativistic projectiles within the energy range of sub-GeV to tens of GeV in straight, bent, periodically bent crystals, and amorphous medium (see the review paper [20] and references therein). The algorithms implemented are also well-documented and their description can be found in Refs. [5,9,17,20,21].

The simulation procedure of the motion an ultra-relativistic particle of energy ε, charge q and mass m is carried out within the framework classical relativistic mechanics. MBN Explorer integrates relativistic equations of motion that are written as follows:

$$\dot{\vec{r}} = \vec{v}, \qquad \dot{\vec{v}} = \frac{1}{m\gamma}\left(\vec{F} - \frac{\vec{v}\left(\vec{v}\cdot\vec{F}\right)}{c^2}\right). \tag{1}$$

Here $\vec{r} = \vec{r}(t)$ and $\vec{v} = \vec{v}(t)$ stand for the particle's position vector and velocity at instant t, $\gamma = \varepsilon/mc^2$ is the relativistic Lorentz factor. The force $\vec{F} = -q\partial U(\vec{r})/\partial\vec{r}$ acting on the projectile is due to electrostatic field created by atoms of the medium.

At each integration step the electrostatic potential $U(\vec{r})$ is computed as the sum of potentials U_{at} of individual atoms

$$U(\vec{r}) = \sum_j U_{\text{at}}(|\vec{r} - \vec{R}_j|). \tag{2}$$

Here $\vec{R}_j$ denotes a position vector of the jth atom. The code allows for the evaluation of atomic potentials using approximations proposed by Molière [22] and Fernandez Pacios [23] The Fernandez Pacios approximation provides basically the same results as frequently used Doyle–Turner scheme [24] but in contrast to the latter it leads to the correct behavior $\propto 1/r$ of U_{at} at small distances (see, e.g., Ref. [25]). More details on the algorithms implemented in MBN Explorer are given [16,20].

In the present paper we consider propagation of 855 MeV electrons through crystalline and amorphous Silicon targets the parameters of which chosen in accordance with the experiment carried out at the MAMI facility [14]. In the case of the oriented crystalline target the simulations have been performed for the electron beam incident on the crystal along the directions probed experimentally as well as along the directions that were not explored in the experimental setup. This allows us to compare the simulated dependencies with the experimentally measured data on the angular distribution of deflected electrons as well as to investigate the evolution of the distribution with variation of the relative orientation of the crystal and the beam. We analyze the transition from the axial to the planar mode and compare our results with the available experimental data presented in Ref [14]. The atomistic approach implemented in MBN Explorer enables simulation the trajectories of charged particles entering a crystal along any chosen direction. Taking advantage of this capability, we have specifically studied the crystal oriented along the $\langle 100 \rangle$ crystallographic axis in the (110) plane.

In Ref. [14] the directions of the incident 855 MeV beam that lead to CSS have been specified in terms of the following two angles: (i) angle Θ_{h} between $\vec{p}_0$ and the $\langle 100 \rangle$ crystallographic axis, and (ii) angle Θ_{v} between $\vec{p}_0$ and the (110) plane. It was estimated that the angle values are to be chosen from the intervals (in mrad):

$$18 < \Theta_{\text{h}} < 43, \qquad 2 < \Theta_{\text{v}} < 4.3. \tag{3}$$

The experiment was carried out using for a 34.2 μm thick silicon crystal. The CSS effect in the angular distribution of the deflected electrons was observed for $\Theta_{\text{h}} = 34.9$ mrad and $\Theta_{\text{v}} = 3$ mrad. The data obtained was compared to the angular distribution measured in 32.76 μm thick amorphous silicon.

In our simulations other values of Θ_{h} and Θ_{v}, that are close to this direction, have been considered. To reproduce the experimental results [14] we have studied the effect of multiple scattering suppression that takes place at certain orientations of the crystalline target. The goal was to determine the necessary conditions for CSS to occur, which typically happens at the incident angle much greater than Lindhard's critical angle, Θ_{L}. Written in terms of the depth U_0 of the continuous interplanar potential Θ_{L} reads $\Theta_{\text{L}} = (2U_0/\varepsilon)^{1/2}$. For a 855 MeV projectile in a (110) channel in a silicon crystal ($U_0 \approx 20$ eV) this estimate provides $\Theta_{\text{L}} \approx 0.22$ mrad.

In the Section below we present and discuss the results of simulations. Basing on the information provided on the experimental setup, the simulations have been carried out for several values of the angles Θ_{h} and Θ_{v} within the intervals specified by Eq. (3). Four sets of the simulations have been performed for the crystalline target. Two sets refer to the fixed value of Θ_{v} (2 and 3 mrad, correspondingly) and Θ_{h} varied within the specified interval. In another pair of sets the value of Θ_{v} was scanned over the interval while Θ_{h} was fixed at 33 and 34.9 mrad.

For each pair $(\Theta_{\text{v}}, \Theta_{\text{h}})$ considered a large number, $N \approx 4 \times 10^4$, of trajectories were simulated. In the course of the simulations the transverse velocity of the particles at the solid target entrance were generated taking into account the Gaussian distributions of the beam particle due to the beam divergencies. The following values of the standard deviations of the divergences of the 855 MeV electron beam at MAMI were used: $\sigma'_{\text{h}} = 70$ and $\sigma'_{\text{v}} = 30$ μrad. General methodology implemented in MBN Explorer to generate particles' trajectories in an atomic environment accounts for randomness in sampling the incoming

projectiles (the key factors here are beam size, divergence and direction with respect to the crystal orientation) as well as in displacement of the lattice atoms from the nodal positions due to thermal vibrations (see Refs. [20,21] for details). As a result, each trajectory corresponds to a unique atomic environment and, therefore, all simulated trajectories are statistically independent and can be analyzed further to quantify the process of interest, the multiple scattering process in particular.

For the sake of comparison, the same number of trajectories have been simulated for 855 MeV electrons passing through amorphous silicon.

To simulate the amorphous environment the following procedure was used. In MBN EXPLORER, when constructing a crystalline structure the position vectors of atomic nuclei are generated with account for random displacement from the nodes due to thermal vibrations corresponding to given temperature T. By introducing unrealistically large value of the root-mean-square thermal vibration amplitude u_T (for example, comparable to the lattice constant a) it is possible to consider large random displacements, i.e. the structure will resemble an amorphous medium. Additionally, one can change the value of the unit cell volume to make the volume density of atoms equal to the volume density in the amorphous medium. To simulate amorphous silicon medium u_T was set to 2 Å. Taking into account that a unit cell of a silicon crystal (with $a = 5.43$ Å) contains 8 atoms, the quoted value of u_T is sufficient enough to ensure randomness of atomic positions in the sample.

3. Results and discussions

The simulated trajectories have been statistically analyzed to provide quantitative data on the particles' distribution in the following two angles[1]:

(i) ϑ_v – the angle between projectile's momentum $\vec{p}$ at the target's exit and the (110) plane;

(ii) ϑ_h – the angle between $\vec{p}$ and the $\langle 100 \rangle$ axial direction.

These planar angles are measured in two perpendicular planes, therefore, the total (round) scattering angle θ is calculated as $\theta = \left(\vartheta_v^2 + \vartheta_h^2\right)^{1/2}$.

The distribution of deflected particles in either of the planar angles can be derived from the distribution in θ. The latter, following Ref. [14], we consider within the framework of the Molière scattering model [22] (see also a paper by Bethe [26]). The details of the derivation are presented in Appendix A. For a planar angle (in the formula below ϑ stands for either of ϑ_v, ϑ_h) the probability distribution function (PDF) that represents the angular distribution function of the particles experienced multiple scattering, can be written as follows:

$$\text{PDF}(\vartheta) = \frac{1}{N}\frac{dN(\vartheta)}{d\vartheta} = \mathcal{A} \sum_{n=0}^{\infty} \left(\frac{\chi_c^2}{2\theta_s^2}\right)^n \frac{1}{n!} \times$$

$$\times \int_0^\infty du\, e^{-u^2/4} \cos\left(u\frac{\vartheta}{\sqrt{2\theta_s^2}}\right)\left(\frac{u^2}{4}\ln\frac{u^2}{4}\right)^n \quad (4)$$

where $dN(\vartheta)$ denotes a number of particles that are scattered by a planar angle lying within the interval $[\vartheta, \vartheta + d\vartheta]$, N is the total number of particles, $\mathcal{A} = 1/\pi\left(2\theta_s^2\right)^{1/2}$ is the normalization factor, and parameter χ_c, dependent on particle's energy and target's thickness, volume density and atomic charge number, is defined in Appendix A, Eq. (A.2). The parameter θ_s is to be determined by fitting the PDF function to the simulated data. To fit the data generated in the simulations with the Molière PDF the Levenberg–Marquardt algorithm [27,28] was implemented. The term with $n = 0$ corresponds to the normal (Gaussian) distributions in which θ_s plays the role of the variance. The terms $n \geq 1$, which provide the correction to the normal distribution, can
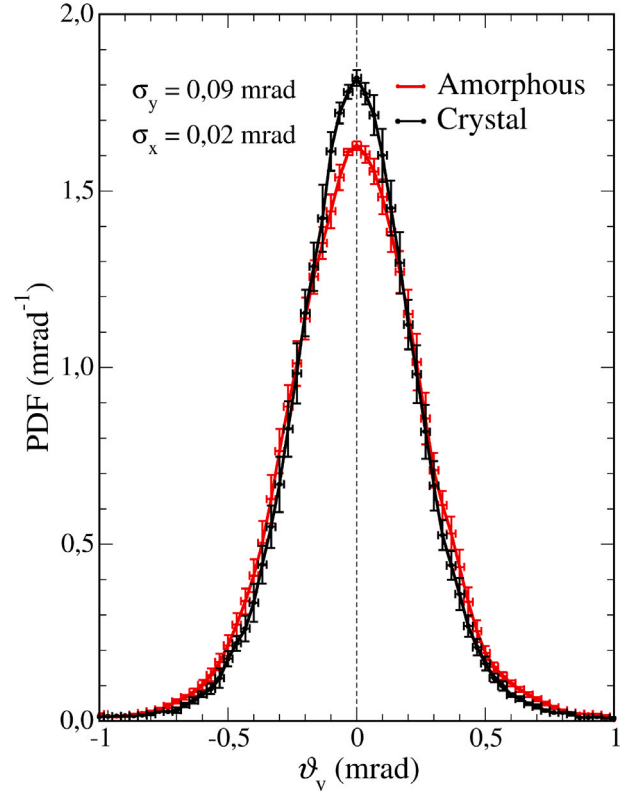
---

[1] In Ref. [14] the notations ϑ_x, ϑ_y are used for the angles ϑ_v, ϑ_h.

Fig. 1. The probability density function (PDF) versus vertical scattering angle ϑ_v plotted for amorphous (red line, filled circles) and crystalline silicon (black line, open circles). The data refer to the incident angles $\Theta_h = 34.9$ mrad and $\Theta_v = 3$ mrad.

be effectively evaluated numerically (see Appendix A for more details). In the fitting procedure the series in (4) were cut off at $n = 12$.

The CSS effect, which was reported in the experiment, has also been observed in our simulations within a specific region characterized by $\Theta_h = 34.9$ mrad and $\Theta_v = 3$ mrad. Fig. 1 compares the PDFs as functions of the vertical scattering angle ϑ_v plotted as histograms using the data obtained from the simulations for the crystalline (black curve with open circles) and amorphous (red curve with filled circles) silicon targets. It can be observed that the PDF values are higher for the crystal silicon compared to the amorphous one in the domain off small scattering angles $|\vartheta_v| \lesssim 0.3$ mrad. Notably, the peak value of the PDF obtained in the simulations is 1.82 mrad^{-1} for the crystal which is slightly higher 1.67 mrad^{-1} for the amorphous target. This suggests that the crystalline silicon exhibits a higher scattering intensity within the specified range of scattering angles compared to the amorphous state. However, it is important to note that our simulation results show a slight broadening of the calculated PDF compared to the experimentally observed data. Numerical PDFs were obtained by generating the organization of the values of $n = 40000$ scattered angles into normalized histograms. The uncertainties present in determining the PDFs of the stands are statistical and are determined by the width of the bins. The best number of bins (all of the same size) describing the PDFs was established using the Rice Rule $2n^{1/3}$. Fig. 1 shows the statistical uncertainties for the scattered angles (width of the bins) and for the population of scattered angles (due to the finite number of the trajectories simulated).

Following Ref. [14], one can consider the difference of PDFs for the crystal and amorphous Si, PDF$_{cr}$-PDF$_{am}$, to quantify further the changes in the angular distributions of electrons passing through the two types of medium. This difference allows one to numerically evaluate the dissimilarity in the PDFs for the two types of medium providing a quantitative measure of the disparity in scattering behavior as well as
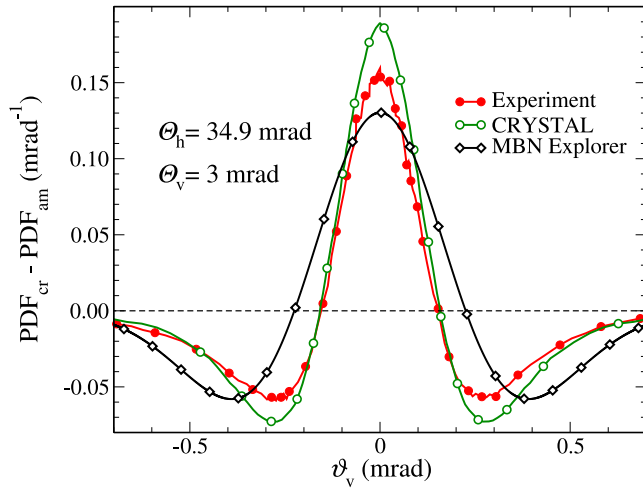
Fig. 2. The difference of PDFs for the beam deflected by the silicon crystal and the amorphous target. Solid red line with filled circles and solid green line with open circles stand for the Experimental data (red line with filled circles) and the results of the CRYSTAL code (green line with open circles) are from Ref. [14]. Black line with open diamonds show the data simulated with MBN Explorer. In all cases the incident angles are $\Theta_v = 3$ mrad and $\Theta_h = 34.9$ mrad.

to gain valuable insights into the structural effects that influence the electron multiple scattering.

Fig. 2 shows the variations in the PDF for the beam deflected by the crystal and amorphous targets. The variations obtained by means of MBN Explorer (black curve with diamonds) are compared to the experimental data (red line with filled circles) and to the results of the simulations with the CRYSTAL code [15] (green line with open circles) both taken from Ref. [14]. All data presented correspond to the incident angles $\Theta_v = 3$ mrad and $\Theta_h = 34.9$ mrad in the case of the crystalline target. The results of the simulations performed with MBN Explorer shown in the figure correspond to the Molière potential. Similar simulations have been performed with the Fernandez Pacios potential (not shown in the figure) and it was that the differences between the two sets of data is less than 0.4%. We consider this as a demonstration of the robustness of our results. All three curves presented in the figure show similar behavior. However, there are some differences between the present simulation and the experimental results regarding, in particular, the width of the central peak of the function.

In our simulations we aimed to investigate the CSS effect over a wide range of the incident angles. Therefore, we have explored values beyond the optimal ranges indicated in Eq. (3) to thoroughly understand the scattering behavior and to assess the robustness of the observed CSS effect.

Following the approach adopted in the experiment [14], we have conducted scans over the incident angles aiming at exploring the variation in the scattering behavior of electrons in crystalline silicon in comparison with the amorphous medium. To this end, two sets of simulations have been carried out. In the first set, the vertical incident angle was fixed at $\Theta_v = 3$ mrad whereas the horizontal angle Θ_h was varied within the interval $[8.7, 52]$ mrad. Similarly, in the second set the angle $\Theta_h = 34.9$ mrad was fixed and the angular distributions was explored in the range $\Theta_v = [1, 10]$ mrad. These scanning parameters allowed us to investigate the angular dependence of the scattering phenomenon and to identify notable trends or/and extrema of the PDFs. For all combinations (Θ_h, Θ_v) considered the simulations were performed using both the Molière and Fernandez Pacios potentials. The PDF obtained were virtually independent on the potential used. The minimum value of θ_s due to the coherent scattering has been found at $\Theta_h = 34.9$ mrad and $\Theta_v = 2$ mrad. This observation provided a crucial

starting point for further analysis and understanding of the scattering behavior in silicon. To quantify the scattering distribution and to derive the PDF for scattered electrons additional scans were performed fixing $\Theta_v = 2$ mrad and varying Θ_h as well as scanning over Θ_v while fixing $\Theta_h = 33$ mrad. These scans allowed us to capture the variations in the PDF as we explored different scattering angles.

Fig. 3 shows the variation of θ_s as a function of one of the incident angles (Θ_h in left graph and Θ_v in right graph) while fixing the second incident angle (see the values indicated at the top of each graph). Solid and dashed lines stand for the crystalline and the amorphous targets, respectively. The results of our simulations are shown as open diamond symbols connected with black lines. Statistical uncertainties due to the finite number of simulated trajectories are indicated with error bars. These uncertainties were obtained by means of the bootstrap algorithm with the Levenberg–Marquardt fitting procedure [27]. The data reported in Ref. [14] are shown with filled circles connected with red lines (the experimental data) and with open circles connected with green lines (the results of simulation with the CRYSTAL code [15]). For the sake of comparison we also present the value of multiple scattering angle calculated for the amorphous silicon by means of Eqs. (34.16), (34.25) and (34.26) from the review by Particle Data Group [29] (see also Appendix B). This value, shown in both graphs with dash-dotted line, corresponds to the mass thickness $T \propto NL$ (N is the volume density, L is the thickness) that one can calculate from the information on the samples used in the experiment indicated Ref. [14]. It is indicated that mass thicknesses of the crystalline and amorphous samples were equal, therefore, $T \propto N_{cr}L_{cr}$ with $L_{cr} = 32.76$ μm as quoted and $N_{cr} = 8/(5.43\,\text{Å})^3 = 5.00 \times 10^{22}$ cm^{-3}.

One can state that there is a close similarity between our results and the experimentally measured data when comparing the profiles of the dependencies $\theta_s(\Theta_h)$ and $\theta_s(\Theta_v)$ for the crystal target. Indeed, the simulations have successfully captured all the essential trends in the dependencies and reproducing the key features observed in the experiment.

To be noted, nevertheless, is a systematic difference in absolute values of the simulated and measured data on θ_s. For both crystalline and amorphous targets the simulations produce higher values with the excess of ca 0.03–0.035 mrad on average.[2] The reason for this discrepancy is unclear. One can speculate that it might be related to some specific algorithm in the statistical processing of the results. For example, it was noted in Ref. [14] that to compare directly the results obtained by means of the CRYSTAL code to the experimental data the former are to be convoluted with the angular distribution of the beam. However, this is definitely not the issue in connection with our methodology since the beam divergence has been explicitly accounted for to randomize "entrance conditions" for the incident particles (in both vertical and horizontal directions). The feature that might be relevant but deserves further analysis concerns the algorithm implemented in MBN Explorer to simulate crystalline and amorphous environment. As mentioned in the last paragraph in Section 2 (see [20,21] for more details) the atomic displacements from the nodal positions are randomly generated. For doing this the normal distribution with the variance equal to u_T is used. This algorithm does not exclude non-physical events when two (or more) atoms will be located in close vicinity to each other. This will result in the (local) increase in the scattering angle which inevitably will affect the multiple scattering angle as well.

---

[2] Also to be noted is that for the amorphous target our result and the experimental data both differ from the commonly used estimate [29] of the multiple scattering angle, see the dash-dotted lines in both graphs in Fig. 3.
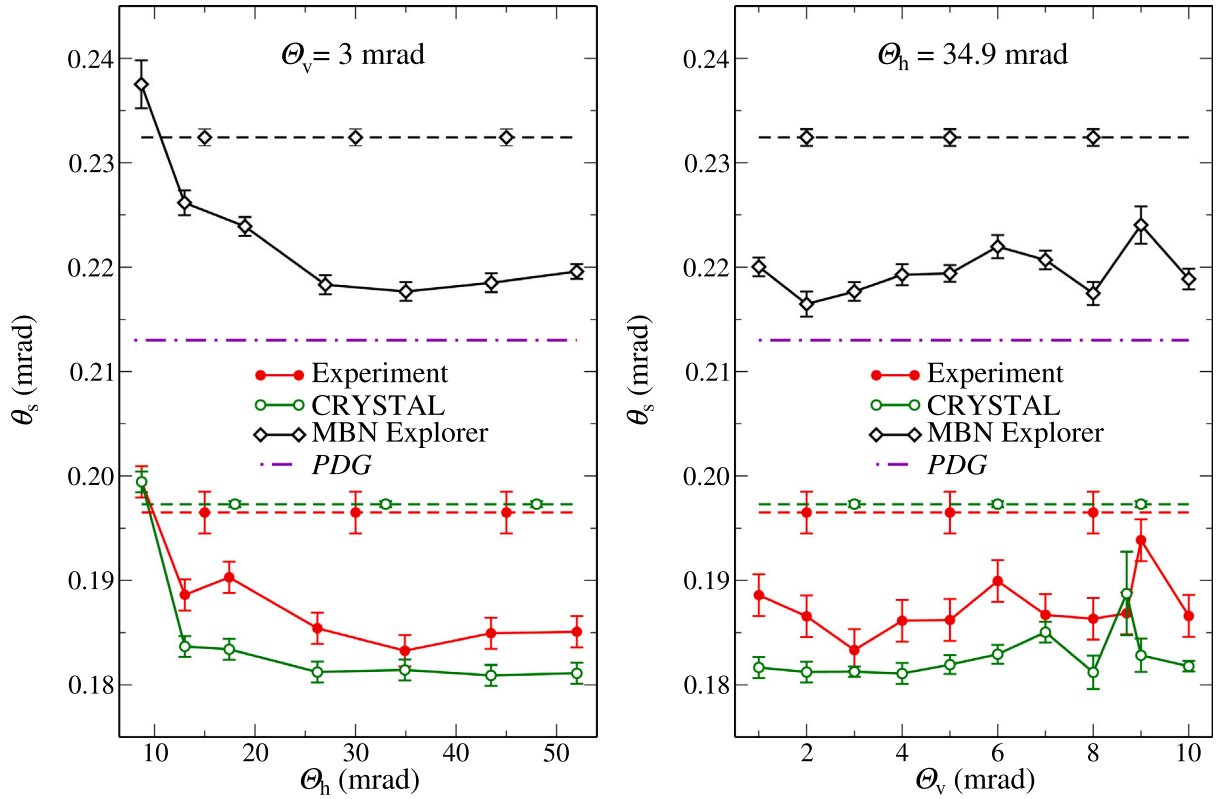
Fig. 3. *Left:* Multiple scattering angle θ_s as a function of the horizontal (left) and vertical (right) incident angles. Solid lines stand for the crystalline target, dashed lines indicate the results for the amorphous medium. Experimental data (red lines, filled circles) and results of simulations with the CRYSTAL code (green lines, open circles) are from Ref. [14]. The results of current simulations (black lines with diamonds) correspond to the Molière potential. For the crystal Si, the incident angles are fixed at: $\Theta_v = 3$ mrad (left) and $\Theta_h = 34.9$ mrad (right). In both graphs the dash-dotted line indicate the rms scattering angle calculated using the formula presented in the review by Particle Data Group (PDG) [29].

4. Conclusions

By means of relativistic all-atom molecular dynamics implemented in the MBN EXPLORER software package the passage of ultra-relativistic electrons through crystalline and amorphous silicon media has been simulated. The parameters of the 855 MeV electron beam and the thickness of the silicon targets utilized in the simulations correspond to those used in the experiment [14] which revealed broad angular anisotropy of multiple scattering in the crystal. For each incident geometry considered a sufficiently large number ($\approx 4 \times 10^4$) of statistically independent trajectories has been generated. The statistical analysis carried out resulted in calculation of the probability distribution functions (PDF) that allowed us to quantify the process of multiple scattering in terms of the planar scattering angles. To double check the results, the simulations and the analysis have been performed employing both the Molière and Fernandez Pacios potentials for the electron–Si-atom interaction. The dependencies of the scattering angle θ_s on both the horizontal Θ_h and vertical Θ_v incident angles turned out to be virtually insensitive to the choice of the potential.

We have observed the differences in angular distributions of electrons deflected by the crystalline and the amorphous targets that were predicted, explained and measured in Ref. [14]. Our results exhibit a high degree of agreement with the experimental data in terms of the profiles of the dependencies $\theta_s (\Theta_h)$ and $\theta_s (\Theta_v)$. We have successfully reproduced values of θ_s for which the phenomenon of coherent scattering suppression was detected and quantified experimentally. In addition, we have examined this phenomenon over a broad range of the incident beam directions.

In terms of absolute values of the scattering angle θ_s there is a systematic difference between the simulated and experimentally measured data. The simulations produce the values of θ_s that are approximately 30–35 μrad higher. As of now, we are uncertain on the origin of this

systematic discrepancy. It might be related difference in the methods of statistical analysis adopted in the current work and in Ref. [14]. We are planning to carry out a study whether this feature might originate from the algorithms implemented in MBN EXPLORER to simulate crystalline and amorphous media (as well as to the phenomena not accounted for; such as, for example, quantum effects in multiple scattering in crystals [30])[3].

Declaration of competing interest

The authors declare that they have no known competing financial interests or personal relationships that could have appeared to influence the work reported in this paper.

Data availability

Data will be made available on request.

---

[3] Note, however, that these effects are negligible in the amorphous medium, see Appendix C.

Acknowledgments

Appendix A. Basic formulae related to the Molière distribution

In what follows we outline the derivation of the 1D distribution function $dP(\vartheta)/d\vartheta$ with respect to a planar scattering angle ϑ, Eq. (4), starting with the Molière 2D distribution function [22] written in terms of the solid scattering angle, $d^2P(\Omega)/d\Omega$, where $d\Omega = \theta d\theta d\phi$ with $\theta \ll 1$ and ϕ being the polar angles. Also presented are auxiliary formulae related to the numerical evaluation of the fitting parameter θ_s by means of the Levenberg–Marquardt algorithm [27,28].

When referring to the Molière distribution formalism the notations introduced in Ref. [26] are used.

Introducing planar scattering angles $\vartheta_x = \theta \cos\phi$ and $\vartheta_y = \theta \sin\phi$, so that $\theta = \left(\vartheta_x^2 + \vartheta_y^2\right)^{1/2}$ and $d\Omega = d\vartheta_x d\vartheta_y$, one writes the 2D distribution as follows:

$$\frac{d^2P(\vartheta_x, \vartheta_y)}{d\vartheta_x d\vartheta_y} = A \sum_{n=0}^{\infty} \left(\frac{\chi_c^2}{2\theta_s^2}\right)^n f^{(n)}(\vartheta_x, \vartheta_y). \tag{A.1}$$

Here

$$\chi_c^2 \approx 4\pi N L \frac{e^4 Z(Z+1)z^2}{\varepsilon^2} \tag{A.2}$$

where $z, p, \upsilon, \varepsilon \approx p\upsilon$ are, respectively, charge of the projectile (in units of the elementary charge e), its momentum, speed and energy calculated in the ultra-relativistic limit; N is the volume density (in $1/\text{cm}^3$) of atoms in the medium, Z is their atomic number, L stands for the target's thickness. Physical meaning of χ_c is that the total probability of a single scattering through an angle greater than χ_c is exactly one.

The functions $f^{(n)}(\vartheta_x, \vartheta_y)$ are given by

$$f^{(n)}(\vartheta_x, \vartheta_y) = \frac{1}{n!} \int_0^\infty J_0\left(u\sqrt{\frac{\vartheta_x^2 + \vartheta_y^2}{2\theta_s^2}}\right) e^{-u^2/4}$$
$$\times \left(\frac{u^2}{4} \ln \frac{u^2}{4}\right)^n u\,du. \tag{A.3}$$

The normalization factor A can be calculated explicitly if both scattering angles $\vartheta_{x,y}$ vary within the infinite interval $[-\infty, +\infty]$. The result reads $A = 1/4\pi\theta_s^2$.

The planar angle θ_s, which enters Eqs. (A.1) and (A.3), is the only free parameter. It is to determined by fitting the simulated or experimentally acquired data with the Molière distribution function.

To derive the 1D distribution one integrates Eq. (A.1) with respect to either variable $\vartheta_{x,y}$ over the infinite interval. Then, using the relation (see, e.g., Eq. 6.554.3 in Ref. [31])

$$\int_{-\infty}^{\infty} J_0\left(a\sqrt{x^2 + b^2}\right) dx = 2\frac{\cos(ab)}{a}, \tag{A.4}$$

one writes the normalized Molière partial distribution function (PDF) with respect to a single planar angle ϑ as follows

$$\text{PDF}(\vartheta; \theta_s) = \frac{dP(\vartheta)}{d\vartheta} = \mathcal{A} \sum_{n=0}^{\infty} \mathcal{B}^n C^{(n)}(\xi) \tag{A.5}$$

$$C^{(n)}(\xi) = \frac{1}{n!} \int_0^\infty du\, e^{-u^2/4} \cos(u\xi) \left(\frac{u^2}{4} \ln \frac{u^2}{4}\right)^n \tag{A.6}$$

where short-hand notations have been introduced:

$$\mathcal{A} = \frac{1}{\pi\sqrt{2\theta_s^2}}, \qquad \mathcal{B} = \frac{\chi_c^2}{2\theta_s^2}, \qquad \xi = \frac{\vartheta}{\sqrt{2\theta_s^2}}. \tag{A.7}$$

Note that PDF depends parametrically on θ_s. This dependence appears explicitly in the normalization factor $\mathcal{A}$, in the factors $\mathcal{B}^n$ and in the argument ξ.

For $n = 0$ the integral is carried out explicitly,[4] $C^{(0)}(\xi) = \sqrt{\pi} \exp\left(-\xi^2\right)$. Therefore, the first term in the series (A.5) corresponds to the Gaussian distribution with variance θ_s. Efficient numerical evaluation of the integrals $C^{(n)}$ with $n \geq 1$ can be achieved by means of the Gauss–Laguerre quadratures (see, e.g., Ref. [28]).

Fitting the data with the distribution (A.5) implies establishing the value of the only free parameter, θ_s, of the distribution. To determine its value one can use the Levenberg–Marquardt algorithm [27,28]. To implement this algorithm an explicit expression for the PDF derivative with respect to θ_s must be known. For the sake of completeness, this formula is written below:

$$\frac{d\text{PDF}}{d\theta_s} = -\frac{1}{\theta_s} \left[\text{PDF} + \mathcal{A} \sum_{n=0}^{\infty} \mathcal{B}^n \left(2nC^{(n)} + \xi D^{(n)}\right)\right] \tag{A.8}$$

where

$$D^{(n)} = \frac{dC^{(n)}}{d\xi} = -\frac{1}{n!} \int_0^\infty u\,du\, e^{-u^2/4} \sin(u\xi) \left(\frac{u^2}{4} \ln \frac{u^2}{4}\right)^n \tag{A.9}$$

Appendix B. Particle data group

A planar rms multiple scattering angle θ_0 for an ultra-relativistic electron/positron ($p\upsilon \approx \varepsilon$) moving in an amorphous medium of density ρ_{am} and thickness L_{am} can be calculated as follows (see Ref. [29], Eq. (34.16)):

$$\theta_0 = \frac{13.6 \,[\text{MeV}]}{\varepsilon} \sqrt{\frac{\rho_{\text{am}} L_{\text{am}}}{X_0}} \left(1 + 0.038 \ln \frac{\rho_{\text{am}} L_{\text{am}}}{X_0}\right). \tag{B.1}$$

Here X_0 is the medium's radiation length (measured in g/cm^2) that determines the mean distance over which a high-energy electron loses all but $1/e$ of its energy by bremsstrahlung, see Eq. (34.25) in [29].

Appendix C. Multiple scattering angle in an amorphous medium

It is well-known, that the small-angle scattering of a charged projectile from an atomic target exhibits significant quantum effects (see, e.g., [32,33]). However, when considering multiple scattering in a macroscopic medium, these effects become negligible. In this auxiliary section we demonstrate this textbook result by direct calculation of an r.m.s. multiple scattering angle of an ultra-relativistic electron of energy ε passing through an amorphous medium. The calculations are performed in the frameworks of (i) plane-wave first Born approximation (see, e.g., [33]), and (ii) classical small-angle scattering approximation, e.g. [34].

The potential energy $U(r)$ of the electron–atom interaction is considered within the Moliére approximation [22]:

$$U(r) = \frac{Ze^2}{r} \sum_{j=1}^{3} a_j\, e^{-b_j r/a_{\text{TF}}}, \tag{C.1}$$

where $a_j = (0.1, 0.55, 0.35)$ and $b_j = (6.0, 1.2, 0.3)$ are the Moliére coefficients, Z is the atomic number and $a_{\text{TF}} = 0.885 Z^{-1/3} a_0$ stands for the Thomas–Fermi radius (a_0 is the Bohr radius).

In an amorphous medium a spatial squared r.m.s. scattering angle $\langle\theta^2\rangle$ is calculated from the formula

$$\langle\theta^2\rangle = n_{\text{am}} L \int \theta^2 \frac{d\sigma_{\text{at}}}{d\Omega} d\Omega = 2\pi n_{\text{am}} L \int_0^{\theta_{\text{max}}} \theta^2 \frac{d\sigma_{\text{at}}}{d\Omega} \theta d\theta \tag{C.2}$$

---

[4] Explicit formula for $C^{(1)}$ is also known, see Refs. [22,26].

Here $d\sigma_{at}/d\Omega$ is the differential cross section of the elastic electron–atom scattering, n_{am} is the volume density of the atoms in the medium, and L is the thickness of the medium in the direction of the incident particle. The upper limit of integration over the polar angle θ is defined as follows (see, e.g., [35]):

$$\theta_{max} \approx \frac{\hbar}{p R_n} \ll 1, \tag{C.3}$$

where $R_n \approx 1.4 A^{1/3} \times 10^{-13}$ cm is the nucleus radius (A denotes the mass number of the nucleus).

The planar r.m.s. scattering angle is given by (see, e.g., Sect. 33 in Ref. [29]):

$$\theta^{rms} = \sqrt{\frac{\langle \theta^2 \rangle}{2}}. \tag{C.4}$$

We use Eqs. (C.1)–(C.4) to calculate θ^{rms} within the two frameworks mentioned above.

C.1. Quantum framework

Cross section of the small-angle elastic scattering of an ultra-relativistic electron from a spherically symmetric atom is (see. e.g. [33]):

$$\frac{d\sigma_{at}}{d\Omega} = \frac{4e^4\varepsilon^2}{c^4} \frac{\left(Z - F(q)\right)^2}{q^4} \approx \frac{4r_0^2}{\gamma^2} \frac{\left(Z - F(q)\right)^2}{\theta^4} \tag{C.5}$$

Here $F(q)$ is the atomic form-factor (i.e. the Fourier image of the electron charge distribution), $q = 2p\sin(\theta/2) \approx p\theta$ is the transferred momentum, $p \approx \varepsilon/c$ is the projectile momentum.

For the Moliére potential one derives $(Z - F(q))/q^2 = Z \sum_{j=1}^{3} a_j \left(q^2 + b_j^2/a_{TF}^2 \right)^{-1}$, so that

$$\frac{d\sigma_{at}}{d\Omega} = \frac{4Z^2 r_0^2}{\gamma^2} \left(\sum_{j=1}^{3} \frac{a_j}{\theta^2 + \theta_j^2} \right)^2 \tag{C.6}$$

where $r_0 = e^2/mc^2 = 2.818 \times 10^{-13}$ cm is the classical electron radius, and $\theta_j = \hbar b_j / p a_{TF}$.

Using the cross section (C.6) in (C.2) one gets the following result for the planar r.m.s. multiple scattering angle within the framework of *quantum mechanics* ("qm"):

$$\theta_{qm}^{rms} \approx \frac{Z r_0}{\gamma} \sqrt{2\pi n_{am} L \left(\ln \frac{a_{TF}}{R_n} - \mathcal{A} \right)} \tag{C.7}$$

where the additive term $\mathcal{A}$ in the brackets is expressed in terms of the Moliére coefficients:

$$\mathcal{A} = \sum_j a_j^2 \left(\ln b_i + 0.5 \right) + \sum_{i>j} \frac{2a_i a_j}{b_i^2 - b_j^2} \left(b_i^2 \ln b_i - b_j^2 \ln b_j \right)$$
$$\approx 0.58. \tag{C.8}$$

C.2. Classical framework

Within the framework of classical mechanics the cross section is calculated as follows (see, e.g. [34])

$$\frac{d\sigma_{at}}{d\Omega} = \frac{\rho(\theta)}{\theta} \left| \frac{d\rho(\theta)}{d\theta} \right|, \tag{C.9}$$

where $\rho = \rho(\theta)$ is the impact parameter as a function of the scattering angle.

In the limit of small scattering angles, the calculation of the dependence $\theta(\rho)$ for an ultra-relativistic particle ($\varepsilon \approx pc$) in the field of the Moliére potential leads to the following result:

$$\theta(\rho) \approx \frac{2}{\varepsilon} \left| \frac{\partial}{\partial \rho} \int_0^\infty U(r) \, dz \right|_{r=\sqrt{\rho^2+z^2}}$$

$$= \frac{2Ze^2}{a_{TF}\varepsilon} \sum_{j=1}^{3} a_j b_j K_1 \left(\frac{b_j}{a_{TF}} \rho \right), \tag{C.10}$$

where $K_1(.)$ is the MacDonald function of the first order.

Using Eqs. (C.9) and (C.10) in (C.2) and noticing that $d\rho(\theta)/d\theta < 0$ one writes the formula for $\langle \theta^2 \rangle$ as follows:

$$\langle \theta^2 \rangle = -2\pi n_{am} L \int_0^{\theta_{max}} \theta^2 \, \rho(\theta) \, \frac{d\rho(\theta)}{d\theta} d\theta$$
$$= 2\pi n_{am} L \int_{\rho_{min}}^\infty \theta^2(\rho) \, \rho \, d\rho \tag{C.11}$$

Here $\rho_{min} \sim R_n$ (see (C.3)). To carry out the integrals containing the factors $K_1(ax)K_1(bx)$ and $K_1^2(ax)$ one makes use of Eqs. (1.12.3.1) and (1.12.3.2) from Ref. [36]. Taking into account that $\rho_{min}/a_{TF} \ll 1$ one gets the following result for the planar r.m.s. multiple scattering angle within the framework of *classical mechanics* ("cl"):

$$\theta_{cl}^{rms} \approx \frac{Z r_0}{\gamma} \sqrt{2\pi n_{am} L \left(\ln \frac{a_{TF}}{R_n} - \mathcal{A} + \ln 2 - C \right)} \tag{C.12}$$

where $\mathcal{A}$ is defined in Eq. (C.8) and $C = 0.577\ldots$ is Euler's constant so that $\ln 2 - C \approx 0.12$.

Comparing Eqs. (C.12) and (C.7) one concludes that with the logarithmic accuracy (i.e. $\ln(a_{TF}/R_n) \gg 1$) both formulae give the same result.

Let us carry out the quantitative estimates for 855 MeV electrons passing through a $L = 32.76$ microns thick amorphous silicon ($Z = 14$, $A = 28$, $n_{am} = 4.71 \times 10^{22}$ cm^{-3}). Using these data in (C.12) and (C.7) one calculates:

$$\theta_{qm}^{rms} \approx 205.5 \,\mu\text{rad} \quad \text{vs.} \quad \theta_{cl}^{rms} \approx 207 \,\mu\text{rad}, \tag{C.13}$$

i.e. the difference between the r.m.s. angles is less than 1 per cent for the parameters considered in the main text.

References

[1] J. Lindhard, Influence of crystal lattice on motion of energetic charged particles, K. Dan. Vidensk. Selsk. Mat. Fys. Medd. 34 (1965) 1.

[2] J.A. Davies, J.D. McIntyre, R.L. Cushing, M. Lounsbury, The range of alkali metal ions of kev energies in aluminum, Can. J. Chem. 38 (1960) 1535.

[3] U.I. Uggerhøj, The interaction of relativistic particles with strong crystalline fields, Rev. Mod. Phys. 77 (2005) 1131.

[4] V.M. Biryukov, Yu.A. Chesnokov, V.I. Kotov, Crystal Channeling and Its Application At High-Energy Accelerators, Springer Science & Business Media, 2013.

[5] Andrey V. Korol, Andrey V. Solov'yov, Walter Greiner, Channeling and Radiation in Periodically Bent Crystals, second ed., in: Springer Series on Atomic, Optical, and Plasma Physics, vol. 69, Springer-Verlag, Berlin Heidelberg, 2014.

[6] A. Mazzolari, M. Romagnoni, R. Camattari, E. Bagli, L. Bandiera, G. Germogli, V. Guidi, G. Cavoto, Bent crystals for efficient beam steering of multi TeV-particle beams. Si crystal, Eur. Phys. J. C 78 (2018) 720.

[7] S.B. Dabagov, Y.P. Gladkikh, Advanced channeling technologies for X-ray applications, Rad. Phys. Chem. 154 (2018) 3.

[8] W. Scandale, G. Arduini, F. Cerutti, M. Garattini, S. Gilardoni, A. Masi, D. Mirarchi, S. Montesano, S. Petrucci, S. Redaelli, R. Rossi, D. Breton, L. Burmistrov, S. Dubos, J. Maalmi, A. Natochii, V. Puill, A. Stocchi, D. Sukhonos, E. Bagli, L. Bandiera, V. Guidi, A. Mazzolari, M. Romagnoni, F. Murtas, F. Addesa, G. Cavoto, F. Iacoangeli, F. Galluccio, A.G. Afonin, M.K. Bulgakov, Yu.A. Chesnokov, A.A. Durum, V.A. Maisheev, Yu.E. Sandomirskiy, A.A. Yanovich, A.A. Kolomiets, A.D. Kovalenko, A.M. Taratin, G.I. Smirnov, A.S. Denisov, Yu.A. Gavrikov, Yu.M. Ivanov, L.P. Lapina, L.G. Malyarenko, V.V. Skorobogatov, G. Auzinger, T. James, G. Hall, M. Pesaresi, M. Raymond, Comprehensive study of beam focusing by crystal devices, Phys. Rev. Accel. Beams 21 (2018) 014702.

[9] A.V. Korol, A.V. Solov'yov, Novel Light Sources beyond Free Electron Lasers, Springer Nature, Switzerland AG, 2022.

[10] G.B. Sushko, A.V. Korol, A.V. Solov'yov, Extremely brilliant crystal-based light sources, Eur. Phys. J. D 76 (2022) 166.

[11] A.V. Korol, A.V. Solov'yov, Atomistic modeling and characterizaion of light sources based on small-amplitude short-period periodically bent crystals, Nucl. Instrum. Methods Phys. Res. B 537 (2023) 1.

[12] A.I. Akhiezer, N.F. Shul'ga, Influence of multiple scattering on the radiation of relativistic particles in amorphous and crystalline media, Sov. Phys. - Uspekhi 30 (1987) 197.

[13] W. Scandale, L.S. Esposito, M. Garattini, R. Rossi, V. Zhovkovska, A. Natochii, F. Addesa, F. Iacoangeli, F. Galluccio, F. Murtas, A.G. Afonin, Yu.A. Chesnokov, A.A. Durum, V.A. Maisheev, Yu.E. Sandomirskiy, A.A. Yanovich, G.I. Smirnov, Yu.A. Gavrikov, Yu.M. Ivanov, M.A. Koznov, M.V. Malkov, L.G. Malyarenko, I.G. Mamunct, J. Borg, T. James, G. Hall, M. Pesaresi, Reduction of multiple scattering of high-energy positively charged particles during channeling in single crystals, Eur. Phys. J. C 79 (2019) 99.

[14] A. Mazzolari, A. Sytov, L. Bandiera, G. Germogli, M. Romagnoni, E. Bagli, V. Guidi, V.V. Tikhomirov, D. De Salvador, S. Carturan, C. Durigello, G. Maggioni, M. Campostrini, A. Berra, V. Mascagna, M. Prest, E. Vallazza, W. Lauth, P. Klag, M. Tamisari, Broad angular anisotropy of multiple scattering in a Si crystal, Eur. Phys. J. C 80 (2020) 63.

[15] A. Sytov, V. Tikhomirov, CRYSTAL simulation code and modeling of coherent effects in a bent crystal at the LHC, Nucl. Instrum. Methods Phys. Res. B 355 (2015) 383.

[16] I.A. Solov'yov, A.V. Yakubovich, P.V. Nikolaev, I. Volkovets, A.V. Solov'yov, MesoBioNano Explorer – A universal program for multiscale computer simulations of complex molecular structure and dynamics, J. Comput. Phys. 33 (2012) 2412.

[17] I.A. Solov'yov, A.V. Korol, A.V. Solov'yov, Multiscale Modeling of Complex Molecular Structure and Dynamics with MBN Explorer, Springer International Publishing, Cham, Switzerland, 2017.

[18] G.B. Sushko, I.A. Solov'yov, A.V. Solov'yov, Modeling MesoBioNano systems with MBN studio made easy, J. Mol. Graph. Model 88 (2019) 247.

[19] MBN explorer and MBN studio software at http://mbnresearch.com.

[20] Andrei V. Korol, Gennady B. Sushko, Andrey V. Solov'yov, All-atom relativistic molecular dynamics simulations of channeling and radiation processes in oriented crystals, Eur. Phys. J. D 75 (2021) 107.

[21] G.B. Sushko, V.G. Bezchastnov, I.A. Solov'yov, A.V. Korol, W. Greiner, A.V. Solov'yov, Simulation of ultra-relativistic electrons and positrons channeling in crystals with MBN Explorer, J. Comput. Phys. 252 (2013) 404.

[22] G. Molière, Theorie der Streuung schneller geladener Teilchen I: Einzelstreuung am abgeschirmten Coulomb-Feld, Z. Naturforsch. A2 (1947) 133.

[23] L. Fernandez Pacios, Analytical density-dependent representation of Hartree–Fock atomic potentials, J. Comput. Chem. 14 (1993) 410.

[24] P.A. Doyle, P.S. Turner, Relativistic Hartree–Fock X-ray and electron scattering factors, Acta Crystallogr. A 24 (1968) 390.

[25] G.V. Dedkov, Interatomic potentials of interactions in radiation physics, Sov. Phys. - Uspekhi 38 (1995) 877.

[26] H.A. Bethe, Molière's theory of multiple scattering, Phys. Rev. 89 (1953) 1256.

[27] D.W. Marquardt, An algorithm for least-squares estimation of nonlinear parameters, J. Soc. Ind. Appl. Math. 11 (1963) 431.

[28] W.H. Press, B.P. Flannery, S.A. Teukolsky, W.T. Vetterling, Numerical Recipies. The Art of Scientific Computing, University Press, Cambridge, 1988.

[29] R.L. Workman others, [Particle Data Group], Review of particle physics, Progr. Theor. Exp. Phys. 2022 (2022) 083C01.

[30] V.V. Tikhomirov, Quantum features of high energy particle incoherent scattering in crystals, Phys. Rev. Accel. Beams 22 (2019) 054501, Erratum; Phys. Rev. Accel. Beams 23 (2020) 039901.

[31] I.S. Gradshtein, I.M. Ryzhik, Table of Integrals, Series, and Products, Elsivier Academic Press, 2014.

[32] L.D. Landau, E.M. Lifshitz, Course of theoretical physics, in: Quantum Mechanics (Non-Relativistic Theory), Vol. 3, Elsevier, Butterworth-Heinemann, Oxford, 1977.

[33] V.B. Berestetskii, E.M. Lifshitz, L.P. Pitaevskii, Course of theoretical physics, in: Quantum Electrodymanics, Vol. 4, Pergamon Press, Oxford, 1982.

[34] L.D. Landau, E.M. Lifshitz, Course of Theoretical Physics, Vol. 1. Mechanics, Buttenworth-Heinemann, Oxford, 1981.

[35] J.D. Jackson, Classical Electrodynamics, Wiley, Hoboken, 1999.

[36] A.P. Prudnikov, Yu.A. Brychkov, O.I. Marichev, Integrals and Series, Vol. 2: Special Functions, Gordon and Breach, New York, 1990.